

# Topological Anderson insulators by latent symmetry

Jing-Run Lin<sup>1</sup>, Shuo Wang<sup>1</sup>, Hui Li<sup>2</sup>, Zheng-Wei Zuo<sup>1\*</sup>

<sup>1</sup>*School of Physics and Engineering, Henan University of Science and Technology, Luoyang 471023, China and*

<sup>2</sup>*Department of Finance and Asset Management,*

*Henan University of Science and Technology, Luoyang 471023, China*

(Dated: January 6, 2025)

Topological Anderson insulators represent a class of disorder-induced, nontrivial topological states. In this study, we propose a feasible strategy to unveil and design the latent-symmetry protected topological Anderson insulators. By employing the isospectral reduction approach from graph theory, we reduce a family of the disordered multi-atomic chains to the disordered dimerized chain characterized by energy-dependent potentials and hoppings, which exhibits the chiral symmetry or inversion symmetry. According to the topological invariants, bulk polarization, and the divergence of localization length of the topological bound edge states in the reduced disordered system, the gapped and ungapped topological Anderson states with latent symmetry could be identified in the original disordered multi-atomic systems. The concept of topological Anderson insulating phases protected by the geometric symmetries and tenfold-way classification is thus extended to the various types of latent symmetry cases. This work paves the way for exploiting topological Anderson insulators in terms of latent symmetries.

*Introduction.*— In condensed matter physics, the topological phases of matter have attracted overwhelming interest over the years due to their exotic bulk phenomena and robust boundary effects[1–8]. Disorders are ubiquitous in real quantum matter, and Anderson localization is disorder-induced localization and plays an important role in quantum matter[9–14]. The presence of disorder can change the topological properties of system. For example, the strong disorder could induce gapped topological Anderson insulators (TAIs) [15–21], ungapped TAIs[22–24], Chern TAIs[25], and topological inverse Anderson insulators[26]. The robustness against disorder is a defining property of the topological quantum states. The physical mechanism of topological edge states in the topological Anderson insulating phases could be explained by effective medium theory[16]. In contrast to the band gap of topological insulators, the TAI states are protected by a mobility gap[27]. In general, TAI with distinct symmetries are characterized by distinct topological invariants. For example, the winding number classifies the chiral or particle-hole symmetries protected TAIs[28–30]. Realization of the higher-order TAIs demands the satisfaction of corresponding point group symmetry[23, 31]. Additionally, the inversion symmetry[32], time-reversal symmetry[15], and average symmetry[33–35] could induce and protect the TAI states. Remarkably, the TAIs with different symmetries have been experimentally observed in disordered cold atomic systems[28], photonic crystals[24, 36–38], and electric circuits[31].

The existence of topological Anderson insulator states beyond the geometric symmetries and tenfold-way classification remains an open question. In this study, we propose a new type of topological Anderson insulating phase, which is protected by latent symmetry. Utilizing the isospectral reduction (ISR) framework from graph theory[39–45], we demonstrate the emergence of

hidden symmetries within reduced systems and exhibition of topological features. The ISR effectively diminishes system size while preserving spectral properties, facilitating the analysis and comprehension of intricate networks and lattice systems. The ISR has proven applicable to diverse physical problems. For instance, a class of accidental degeneracies can be explained by the latent symmetry of an isospectral effective Hamiltonian, which is derived through subsystem partitioning[46]. The latent symmetry within the lattice unit cell offers valuable insights to analyze and design perfectly flat band structures[47]. Upon performing an ISR, an oversized system lacking apparent symmetries may reduce to the Su-Schrieffer-Heeger (SSH) model with energy-dependent hopping amplitudes[48]. This approach could also dramatically simplify a variety of complex fractal systems and reveal the topological boundary and corner states[49]. A family of seemingly complicated two-dimensional models by the IRS method can be transformed into an energy-dependent Haldane models[50]. Moreover, various latent symmetries with the ISR approach play a pivotal role in distinctly topological schemes, manifesting in systems such as zigzag granular chains exhibiting latent mirror symmetry[51], higher-order topological crystalline insulators with latent rotation symmetry[52], acoustic wave systems possessing latent mirror symmetry[53], non-Hermitian models demonstrating emergent sublattice symmetry[54], and quasiperiodic network models characterized by hidden self-duality[55].

In the following, we utilize the ISR to one-dimensional (1D) general tight-binding models with latent symmetries, such that they reduce to the disordered dimerized models. This framework enables the revelation and characterization of various topological Anderson insulating phases, including both gapped and ungapped TAIs, protected by latent chiral symmetry and inversion sym-

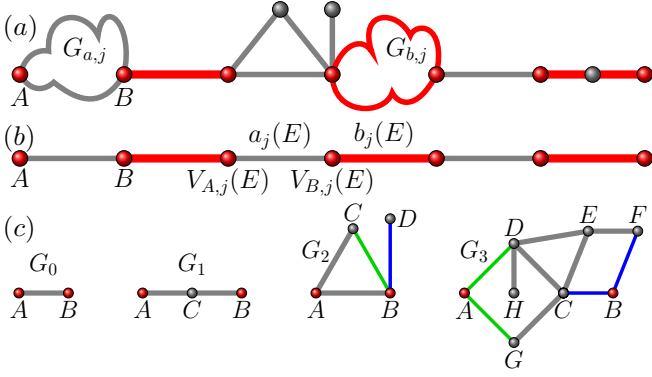


FIG. 1. The arbitrary lattice building blocks  $G_{a,j}$  for intracell and lattice building blocks  $G_{b,j}$  for intercell are connected at vertices  $A$  and  $B$ , as illustrated by the possible lattice building blocks in (a). (b) The ISR of the Hamiltonian in (a) over the set  $S = \{A, B\}$  yields the onsite potentials at lattice sites  $A$  and  $B$  as  $V_{A,j}(E)$  and  $V_{B,j}(E)$ , respectively. The intracell hopping amplitudes are given by  $a_j(E)$ , and the intercell hopping amplitudes by  $b_j(E)$ . (c) A series of lattice building blocks  $G_0, G_1, G_2$ , and  $G_3$  with two cospectral vertices  $S = \{A, B\}$  forming a latently symmetric site pair.

metry. These phases are identified through topological invariants and the divergence of localization length exhibited by topological edge states. This work elucidates and predicts the existence of latent-symmetry protected topological Anderson insulating phases in 1D disordered multi-atomic chains.

*Setup.*— We investigate general 1D models with complex lattice structures [see Fig.1(a)], particularly in the presence of disorder, such as randomness in hopping amplitudes. Due to their inherent complexity and the existence of disorder, the conventional topological tools such as symmetry-indicator theory[56, 57], topological quantum chemistry[58, 59], and spin group theory[60–62], can not characterize and classify the topological features of current systems. As a substitute, we use an ISR approach to reduce the Hamiltonian of system into an effective Hamiltonian of the well-defined topological systems after a suitable reduction which preserves the eigenvalue spectrum to unearth the latent symmetry. The Hilbert space of Hamiltonian  $H$  can be partitioned in a structure set  $S$  (for example lattice sites  $A, B$ ) and its complement  $\bar{S}$ .  $H$  has the block matrix form

$$H = \begin{bmatrix} H_{SS} & H_{\bar{S}S} \\ H_{S\bar{S}} & H_{\bar{S}\bar{S}} \end{bmatrix}. \quad (1)$$

The ISR reduced effective Hamiltonian  $R_S(H, E)$  of  $H$  over the set  $S = \{A, B\}$  is then defined[39]

$$\mathcal{R}_S(H, E) = H_{SS} + H_{S\bar{S}}(EI - H_{\bar{S}\bar{S}})^{-1}H_{\bar{S}S}, \quad (2)$$

where  $I$  is the identity matrix and the matrix  $H_{\bar{S}\bar{S}} - EI$  is invertible.

Generally, we select a set  $S$  with lattice sites  $A$  and  $B$ , defined as  $S = \{A, B\}$ , we can express the isospectral effective Hamiltonian of dimerized chain derived by subsystem partitioning as (set lattice constant  $a = 1$  of  $N$  unit cells):

$$\begin{aligned} \mathcal{R}_S(H, E) = & \left[ \sum_j^N a_j(E) c_{A,j}^\dagger c_{B,j} + \sum_j^{N-1} b_j(E) c_{B,j}^\dagger c_{A,j+1} \right. \\ & \left. + h.c. \right] + \sum_j^N (V_{A,j}(E) c_{A,j}^\dagger c_{A,j} + V_{B,j}(E) c_{B,j}^\dagger c_{B,j}), \quad (3) \end{aligned}$$

where the onsite potentials of lattice sites  $A(B)$  are  $V_{A,j}(E)(V_{B,j}(E))$ , the intracell hopping amplitudes are  $a_j(E)$ , and intercell hopping amplitudes are  $b_j(E)$ . Generally, the potential and hopping are energy-dependent. Here,  $c_{\alpha,j}^\dagger(c_{\alpha,j})$  denotes the creation (annihilation) operator at site  $\alpha$  ( $\alpha$  stands for the lattice sites  $A$  or  $B$ ) of the  $j$ -th unit cell. For any 1D model with an arbitrary intracell lattice building blocks  $G_{a,j}$  and intercell lattice building blocks  $G_{b,j}$ , as long as adjacent  $G_{a,j}$  and  $G_{b,j}$  share exactly one common lattice site (either  $A$  or  $B$ ), the Hamiltonian of the dimerized chain [illustrated in Fig.1(b)] described above can be obtained through the ISR.

The graph of lattice building blocks is depicted in Fig1(c). The structures  $G_0$  and  $G_1$  obey the inversion symmetry, but there is no obvious structural symmetry of  $G_2$  and  $G_3$ . Performing an isospectral graph reduction[39] over the red sites (lattice sites  $A$  and  $B$ ), we can transform  $G_2$  and  $G_3$  into structures that exhibit the same structural symmetry as  $G_0$ . As a result, the system of lattice sites  $A$  and  $B$  acquires latent inversion symmetry on  $G_2$  and  $G_3$ .

For the isospectral effective Hamiltonian Eq.(3), if the onsite potentials satisfy  $V_{A,j} = V_{B,j} = V$ , then  $\hat{\mathcal{R}}_S(H) - VI$  takes on the mathematical form of the disordered SSH model with chiral symmetry, that is, this original 1D chain has latent chiral symmetry. The chiral symmetry that acts on the isospectral effective Hamiltonian can be expressed in position space as

$$\Gamma = \sum_{j=1}^N c_j^\dagger \sigma_3 c_j, \quad (4)$$

and it follows that  $\{\Gamma, (\mathcal{R}_S(H) - VI)\} = 0$ , where  $\sigma_\beta$ , for  $\beta = 1, 2, 3$ , denotes the Pauli matrices acting on the two orbitals  $\{A, B\}$  in each unit cell.

In a disordered SSH chain with chiral symmetry, the topological number  $\mathcal{Q}_f$  can recognize the topological properties at filling factor  $f$ , which is given by [63, 64]:

$$\mathcal{Q}(E_f) = \frac{1}{2} [1 - \text{sign} \{ \prod_{j=1}^N a_j(E_f)^2 - \prod_{j=1}^N b_j(E_f)^2 \}]. \quad (5)$$

As we know that the divergence of the localization length for the topological localized zero-energy edge modes is accompanied by the topological phase transition of the disordered SSH model with chiral symmetry [19]. The Schrödinger equation for the zero-energy eigenstate  $\psi$  in this case reads  $(\hat{\mathcal{R}}_S(H, E_f) - VI)\psi = 0$ , where  $E_f$  is the energy of Hamiltonian  $H$  at filling factor  $f$ . We numerically compute the localization length  $\Lambda$  of the eigenvector of the edge states using a numerical transfer matrix method[65]. We can obtain inverse of the localization length for the zero-energy mode as (in the thermodynamic limit  $N \rightarrow \infty$ ):

$$\Lambda(E_f)^{-1} = \left| \lim_{N \rightarrow \infty} \frac{1}{N} \sum_{j=1}^N (\ln |b_j(E_f)| - \ln |a_j(E_f)|) \right|, \quad (6)$$

in which  $\Lambda^{-1}$  is inverse of the localization length at filling factor  $f$ .

On the other hand, when the onsite potentials and hopping amplitudes exhibit inversion symmetry ( $V_{A,j} = V_{B,N+1-j}$ ,  $a_j = a_{N+1-j}$ ,  $b_j = b_{N+1-j}$ ), the isospectral effective Hamiltonian  $\hat{\mathcal{R}}_S(H)$  corresponds to a disordered 1D inversion-symmetric chain. Here, the inversion center is located at  $\mathcal{X} = N/2 + 1/2$  ( $\mathcal{X} = N/2$ ) under periodic boundary condition (PBC), when the unit cell number  $N$  is even (odd).

Here, we use polarization[66] in real space as the topological invariant to characterize the topological phase transitions in the disordered multi-atomic chain with latent inversion symmetry, which is defined as:

$$P_0 = \sum_n^N \left( \frac{1}{2\pi} \text{Im} \ln \xi_n \right). \quad (7)$$

The set of eigenvalues  $\{\xi_n\}$  is given by the position operator projected onto the occupied states ( $X_P = P_{occ} X P_{occ}$ ), where  $X = \sum_j^N e^{2\pi i j} (|A, j\rangle\langle A, j| + |B, j\rangle\langle B, j|)$  is position operator,  $P_{occ} = \sum_{occ} |\psi_n\rangle\langle\psi_n|$  is the projector in the subspace of occupied states, with  $|\psi_n\rangle$  being the eigenstate of  $\hat{\mathcal{R}}_S(H, E^n)\psi_n = E^n\psi_n$ . The theorem in [67] states that ISR preserves the eigenvectors corresponding to the eigenvalues of  $H$ . Specifically, the eigenvectors of  $\hat{\mathcal{R}}_S(H)$  could be obtained by projecting the eigenvectors of  $H$  onto the set  $S$ , meaning that they consist of the components of the eigenvectors of  $H$  indexed by  $S$ .

Thus, the topological information of the reduced Hamiltonian comes from that of the larger Hamiltonian that is latent. This uncovering of topological information in the reduced Hamiltonian allows us, via the extension of these classical methods, to characterize the topological phases of complex systems.

*Tetra-atomic chains with latent chiral symmetry.*— To give an explicit demonstration of the isospectral reduction approach, we firstly investigate the case where  $G_{a,j}$

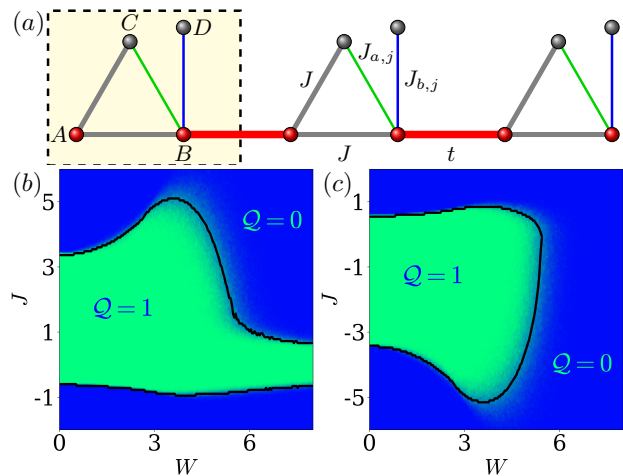


FIG. 2. (a) The tetra-atomic chain consists of four sites with intracell hopping amplitudes  $J$  (gray solid line),  $J_a$  (green solid line), and  $J_b$  (blue solid line). (b,c) The phase diagram at fillings 1/4 and 3/4 of the tetra-atomic chain for correlated random disorders with  $t = 1$ .

and  $G_{b,j}$  in a 1D chain are each fixed to a specific lattice building block. As shown in Fig.2(a), the lattice building block for intracell is  $G_2$ , and  $G_0$  is the lattice building block for intercell (The  $G_1$ , and  $G_0$  are set as the lattice building block case of the intracell and intercell, which can be found in Supplementary Material[68]). We could write the tight-binding model in real space as

$$H_Q = \sum_j^N [Jc_{A,j}^\dagger(c_{B,j} + c_{C,j}) + c_{B,j}^\dagger(J_{a,j}c_{C,j} + J_{b,j}c_{D,j})] + \sum_j^{N-1} tc_{B,j}^\dagger c_{A,j+1} + h.c.. \quad (8)$$

where the intercell hopping amplitude is  $t$ , the intracell hopping amplitudes are  $J, J_{a,j} = J_0 + W\omega_j$ , and  $J_{b,j} = \sqrt{J^2 - J_{a,j}^2}$ , where  $J_0 = J/\sqrt{2}$ .

By inspection, the system given by Eq.(8) hosts a latent chiral symmetry, which is revealed through the ISR. For isospectral effective Hamiltonian with  $a_j = J + J(J_0 + W\omega_j)/E$ ,  $b_j = t$ , and  $V = J^2/E$ , the inverse of the localization length for the topological edge states is

$$\Lambda^{-1} = \left| \ln \left[ \frac{2Et|2EJ + 2JJ_0 - JW| \left( \frac{EJ + JJ_0}{JW} - \frac{1}{2} \right)}{|2EJ + 2JJ_0 + JW| \left( \frac{EJ + JJ_0}{JW} + \frac{1}{2} \right)} \right] + 1 \right|. \quad (9)$$

We investigate the topological numbers  $Q$  of the tetra-atomic chain with fixed  $t = 1$  at fillings 1/4 and 3/4, which are shown in Fig.2(b,c). We also plot the divergence points of localization length  $\Lambda$  of zero-energy modes as the black solid lines. The computations of phase diagrams are done for  $N = 200$  and averaged over  $N_c = 100$

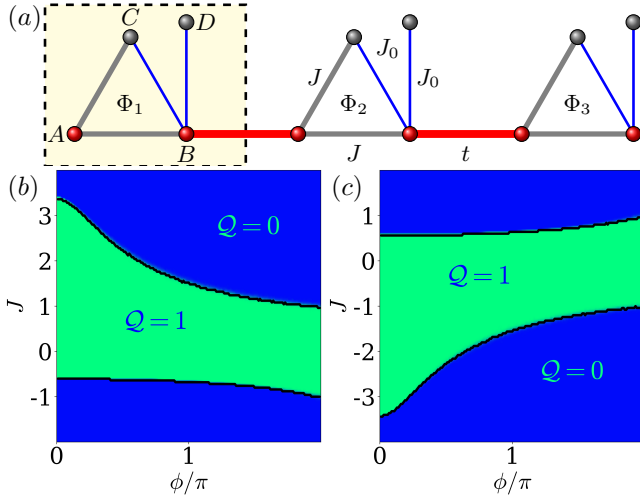


FIG. 3. (a) Schematics of the tetra-atomic chain with random flux. The phase diagram at fillings 1/4 (b) and 3/4 (c) of the tetra-atomic chain for random flux with  $t = 1$ .

disorder configurations. These results indicate that the changes of topological number  $\mathcal{Q}$  are accompanied by the divergence of localization length, which implies the topological phase transitions. In the green region, the system is in the latent chiral symmetry protected topological Anderson insulator phase.

Next, we further investigate the topological Anderson insulator states induced by the random flux in tetra-atomic chain [illustrated in Fig.3(a)], where the random flux could induce the topological phase transitions [69, 70]. This disordered chain could be described by the following tight-binding Hamiltonian

$$H_Q = \sum_j^N [J e^{i\Phi_j} c_{A,j}^\dagger (c_{B,j} + c_{C,j}) + J_0 (c_{B,j}^\dagger c_{C,j} + c_{B,j}^\dagger c_{D,j})] + \sum_j^{N-1} t c_{B,j}^\dagger c_{A,j+1} + h.c., \quad (10)$$

where the intercell hopping amplitude is  $t$ , the intracell hopping amplitudes are  $J$  and  $J_0 = J/\sqrt{2}$ . For convenience, we choose the random flux  $\Phi_j = \phi\omega_j$  with disorder strength  $\phi$  and uniform disorder distribution  $\omega_j \in [-1/2, 1/2]$ , in units of the magnetic flux quantum  $\phi_0 = hc/e$ .

For this disordered tetra-atomic chain model with random flux after performing ISR, the energy-dependent intracell coupling is  $a_j = J e^{i\phi\omega_j} + J J_0/E$ , the intercell coupling is  $b_j = t$ , and the energy-dependent on-site potential is  $V = J^2/E$ . This model features a latent chiral symmetry:  $\Gamma(\mathcal{R}_S(H_Q) - VI)\Gamma^{-1} = -(\mathcal{R}_S(H_Q) - VI)$ .

By calculating the disorder-averaged real-space topological number  $\mathcal{Q}$  for the system of  $N = 200$  on the  $W-J$  plane over  $N_c = 100$  disorder configurations, we obtain

the topological phase diagram shown in Fig.3(b,c). It is easy to see that the random flux can induce TAIs with latent chiral symmetry. In the clean limit  $\Phi = 0$ , the system is in the trivial phase with  $\mathcal{Q} = 0$  at filling 1/4 for intracell hopping  $J \lesssim -0.6$  ( $J \gtrsim 0.6$  at filling 3/4) in Fig.3b (c). Interestingly, there exists nontrivial  $\mathcal{Q} = 1$  phase in the intracell hopping  $J \lesssim -0.6$  ( $J \gtrsim 0.6$  at filling 3/4) region with moderate disorder strength, indicating the existence of TAIs induced by the random flux. The black lines in Fig.3(b,c) stand for the divergence points of localization length  $\Lambda$  of the zero-energy states of the Hamiltonian matrix  $\mathcal{R}_S(H_Q) - VI$ , which are in accordance with the topological phase transitions.

*Octatomic chain with latent inversion symmetry*— Having established the features of the multi-atomic chain with latent chiral symmetry and its topological invariants in position space, we discuss the effects of disorder on the multi-atomic chain with latent inversion symmetry. As shown in Fig.4(a), the lattice building block for intracell is  $G_3$ , and  $G_0$  is the lattice building block for intercell. This Hamiltonian of octatomic chain in real space could be written as

$$H_O = \sum_j^N [J_{a,j} c_{A,j}^\dagger (c_{D,j} + c_{G,j}) + J_{b,j} c_{B,j}^\dagger (c_{C,j} + c_{F,j}) + J c_{C,j}^\dagger (c_{D,j} + c_{E,j} + c_{G,j}) + J c_{D,j}^\dagger (c_{E,j} + c_{H,j}) + J c_{E,j}^\dagger c_{F,j}] + \sum_j^{N-1} t c_{B,j}^\dagger c_{A,j+1} + h.c., \quad (11)$$

where the intercell hopping amplitude is  $t$ , the intracell hopping amplitudes are  $J, J_{a,j} = J + W\omega_{a,j}$ , and  $J_{b,j} = J + W\omega_{b,j}$ . The random numbers are restricted by  $\omega_{a,j} = \omega_{b,N+1-j}$  for each disorder configurations, which leads to that onsite potentials  $V_{A,j} = V_{B,N+1-j}$  and intracell hopping amplitudes  $J_j = J_{N+1-j}$  are constrained to ensure the inversion symmetry. Then the reduced effective Hamiltonian  $\mathcal{R}_S(H_O, E)$  takes on the mathematical form of the disordered inversion-symmetric chain, where the inversion center is chosen about  $\mathcal{X} = N/2 + 1/2$  ( $N$  is even). The inversion operator for inversion center can be expressed in real space as follows:

$$I_{\mathcal{X}} = \sum_{j=1}^N c_{N+1-j}^\dagger \sigma_1 c_j. \quad (12)$$

We can show that  $[I_{\mathcal{X}}, \hat{\mathcal{R}}_S(H_O)] = 0$ . Thus, we can obtain the real space bulk polarization by energy-dependent



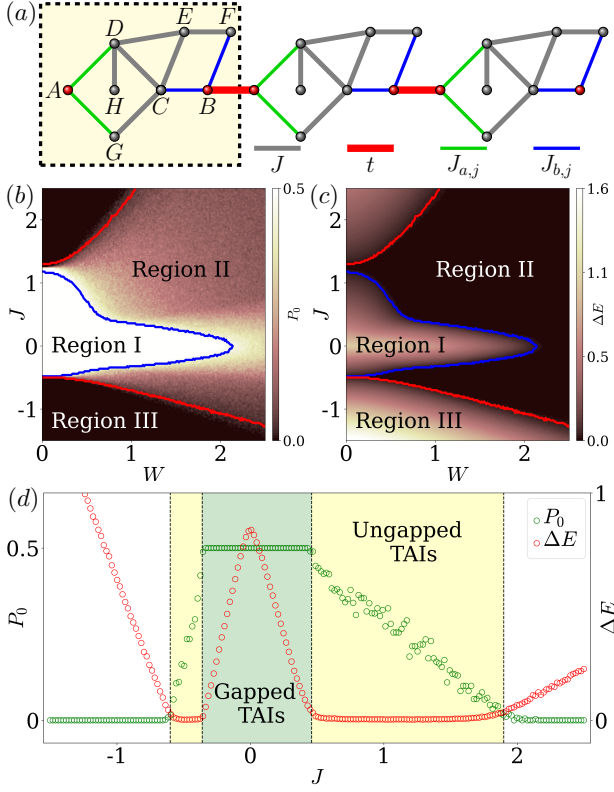


FIG. 4. (a) The octatomic chain is composed of eight lattice points per unit cell. The intercell hopping amplitude is  $t$ , and the intracell hopping amplitudes are  $J$ ,  $J_{a,j}$ , and  $J_{b,j}$ . (b) Topological invariant  $P_0$  and (c) bulk energy gap  $\Delta E$  in the  $(W, J)$  plane at filling  $1/8$  with  $t = 1$ ,  $N = 200$ , and  $N_c = 100$ . The red (blue) solid line indicates the phase boundary determined by  $\Delta E = 3 \times 10^{-2}$ . (d) The energy gap  $\Delta E$  and bulk polarization  $P_0$  as a function of  $J$  are presented when the system size  $N = 200$ ,  $N_c = 100$ ,  $t = 1$ ,  $W = 0.65$ .

terms:

$$\begin{cases} a_j = \frac{2E^2 J J_{a,j} J_{b,j}}{E^4 - E^3 J - 4E^2 J^2 + EJ^3 + J^4} \\ b_j = t \\ V_{A,j} = \frac{2E J_{a,j}^2 (E^2 - EJ - J^2)}{E^4 - E^3 J - 4E^2 J^2 + EJ^3 + J^4} \\ V_{B,j} = \frac{2E J_{b,j}^2 (E^2 - EJ - J^2)}{E^4 - E^3 J - 4E^2 J^2 + EJ^3 + J^4} \end{cases} \quad (13)$$

from this disordered octatomic chain, where energy-dependent terms satisfy inversion symmetry.

In Fig.4(b), we categorize the topological phases region into two distinct phases: the gapped TAIs in region I and the ungapped TAIs in region II. This categorization is based on whether the  $N$ th and  $(N + 1)$ th eigenvalues are degenerate. For a given disorder configuration denoted by the label  $s$ , the corresponding disorder-averaged bulk

gap  $\Delta E$  under PBC is given by

$$\Delta E = \frac{1}{N_c} \sum_{j=1}^{N_c} |E_{s,N+1} - E_{s,N}|. \quad (14)$$

From this we can plot disorder-averaged energy gap on the  $W - J$  plane which is shown in Fig.4(c).

Figure 4(b) illustrates that the disorder-averaged value of  $P_0$  is quantized in region I and nontrivial up to the boundary of fluctuation onset value (blue solid line). Because the bulk polarization fluctuates between a set of quantized values which alters the disorder-averaged value of bulk polarization in the ungapped TAI region. Comparing Fig.4(b) and Fig.4(c), it is obvious that the bulk polarization  $P_0$  fluctuations are connected to the closing of the disorder-averaged energy spectral gap. When the bulk energy spectral gap closes, the disorder-averaged value of the bulk polarization  $P_0$  is no longer quantized in region II of the phase diagram. In other words, as long as the energy gap does not close, the system still remains in the gapped TAI state. It should be noted that the bulk polarization  $P_0$  for a single disorder configuration is still quantized. When the system evolves cross the phase boundary (red solid line), there is a transition in the value of  $P_0$  becoming trivial and equaling 0. Beyond the blue solid line, the region within the red solid line corresponds to the energy gap  $\Delta E \leq 3 \times 10^{-2}$ . In region III of Fig.4(b), the system is in a trivial phase and the energy gap opens again.

Hereafter, we take the evolution of polarization  $P_0$  and  $\Delta E$  with couplings  $J$  at  $W = 0.65$  as an example. As shown in Fig.4(d), we categorize the region of  $W = 0.65$  into three distinct phases: the trivial insulators ( $J \lesssim -0.6$  and  $1.9 \lesssim J$ , white shaded region), the gapped TAIs ( $-0.36 \lesssim J \lesssim 0.46$ , green shaded region) and the ungapped TAIs ( $-0.6 \lesssim J \lesssim -0.36$  and  $0.46 \lesssim J \lesssim 1.9$ , yellow shaded region). When  $J \approx -0.36$ , the polarization changed progressively from  $P_0 = 0$  to  $P_0 = 1/2$ , which clearly reveals that disorder induces the topological phase transition. The system will maintain in TAI phase until  $J \approx 1.9$ , and then return to the trivial phase. The computations of Fig.4(d) were done for  $N = 200$  and averaged over  $N_c = 100$  disorder configurations. From the above discussion, we show the possibility of the disorder-driven topological phases protected by latent inversion symmetry including the gapped and ungapped TAIs.

*Summary and outlook*— In short, we propose a theoretical framework leveraging the isospectral reduction approach from graph theory to uncover topological Anderson insulator states protected by latent symmetries in disordered multi-atomic chains. Taking the tetra-atomic chain and octatomic chain as representative examples, we demonstrate that this reduction approach simplifies complex lattice systems of many degrees of freedom while pre-

serving their essential topological features. Latent symmetries and topological properties emerge clearly within the reduced systems, enabling characterization of the original systems' topological phases through topological invariants and edge states. Furthermore, these latent symmetry protected topological phases can be directly verified in current experimental techniques such as cold atoms[28], photonic crystals[36], and topoelectrical circuits[31]. Our work provides valuable insights for discovering and designing the latent symmetry protected topological Anderson insulators.

*Acknowledgements.*—This work was supported by the National Natural Science Foundation of China (Grant No. 12074101) and the Natural Science Foundation of Henan (Grant No. 212300410040).

---

\* zuozw@haust.edu.cn

- [1] M. Z. Hasan and C. L. Kane, *Colloquium* : Topological insulators, *Rev. Mod. Phys.* **82**, 3045 (2010).
- [2] X.-L. Qi and S.-C. Zhang, Topological insulators and superconductors, *Rev. Mod. Phys.* **83**, 1057 (2011).
- [3] B. A. Bernevig and T. L. Hughes, *Topological insulators and Topological Superconductors* (Princeton University Press, 2013).
- [4] S. R. Elliott and M. Franz, *Colloquium* : Majorana fermions in nuclear, particle, and solid-state physics, *Rev. Mod. Phys.* **87**, 137 (2015).
- [5] J. K. Asbóth, L. Oroszlány, and A. Pályi, *A Short Course on Topological Insulators* (Springer, 2016).
- [6] X.-G. Wen, Colloquium: Zoo of quantum-topological phases of matter, *Rev. Mod. Phys.* **89**, 041004 (2017).
- [7] E. J. Bergholtz, J. C. Budich, and F. K. Kunst, Exceptional topology of non-Hermitian systems, *Rev. Mod. Phys.* **93**, 015005 (2021).
- [8] R. Moessner and J. E. Moore, *Topological Phases of Matter* (Cambridge University Press, 2021).
- [9] P. W. Anderson, Absence of diffusion in certain random lattices, *Phys. Rev.* **109**, 1492 (1958).
- [10] E. Abrahams, P. W. Anderson, D. C. Licciardello, and T. V. Ramakrishnan, Scaling theory of localization: Absence of quantum diffusion in two dimensions, *Phys. Rev. Lett.* **42**, 673 (1979).
- [11] P. A. Lee and D. S. Fisher, Anderson Localization in Two Dimensions, *Phys. Rev. Lett.* **47**, 882 (1981).
- [12] R. Gade, Anderson localization for sublattice models, *Nucl. Phys. B* **398**, 499 (1993).
- [13] F. A. B. F. De Moura and M. L. Lyra, Delocalization in the 1D Anderson Model with Long-Range Correlated Disorder, *Phys. Rev. Lett.* **81**, 3735 (1998).
- [14] F. M. Izrailev and A. A. Krokhnin, Localization and the Mobility Edge in One-Dimensional Potentials with Correlated Disorder, *Phys. Rev. Lett.* **82**, 4062 (1999).
- [15] J. Li, R.-L. Chu, J. K. Jain, and S.-Q. Shen, Topological Anderson insulator, *Phys. Rev. Lett.* **102**, 136806 (2009).
- [16] C. W. Groth, M. Wimmer, A. R. Akhmerov, J. Tworzydło, and C. W. J. Beenakker, Theory of the topological Anderson insulator, *Phys. Rev. Lett.* **103**, 196805 (2009).
- [17] H.-M. Guo, G. Rosenberg, G. Refael, and M. Franz, Topological Anderson insulator in three dimensions, *Phys. Rev. Lett.* **105**, 216601 (2010).
- [18] Y. Xing, L. Zhang, and J. Wang, Topological Anderson insulator phenomena, *Phys. Rev. B* **84**, 035110 (2011).
- [19] I. Mondragon-Shem, T. L. Hughes, J. Song, and E. Prodan, Topological criticality in the chiral-symmetric AIII class at strong disorder, *Phys. Rev. Lett.* **113**, 046802 (2014).
- [20] A. Altland, D. Bagrets, L. Fritz, A. Kamenev, and H. Schmiedt, Quantum criticality of quasi-one-dimensional topological Anderson insulators, *Phys. Rev. Lett.* **112**, 206602 (2014).
- [21] Z. Xiao, K. Kawabata, X. Luo, T. Ohtsuki, and R. Shindou, Anisotropic topological Anderson transitions in chiral symmetry classes, *Phys. Rev. Lett.* **131**, 056301 (2023).
- [22] D. Xu, J. Qi, J. Liu, V. Sacksteder, X. C. Xie, and H. Jiang, Phase structure of the topological Anderson insulator, *Phys. Rev. B* **85**, 195140 (2012).
- [23] Y.-B. Yang, K. Li, L.-M. Duan, and Y. Xu, Higher-order topological Anderson insulators, *Phys. Rev. B* **103**, 085408 (2021).
- [24] M. Ren, Y. Yu, B. Wu, X. Qi, Y. Wang, X. Yao, J. Ren, Z. Guo, H. Jiang, H. Chen, X.-J. Liu, Z. Chen, and Y. Sun, Realization of Gapped and Ungapped Photonic Topological Anderson Insulators, *Phys. Rev. Lett.* **132**, 066602 (2024).
- [25] Y. Su, Y. Avishai, and X. R. Wang, Topological Anderson insulators in systems without time-reversal symmetry, *Phys. Rev. B* **93**, 214206 (2016).
- [26] Z.-W. Zuo, J.-R. Lin, and D. Kang, Topological inverse Anderson insulator, *Phys. Rev. B* **110**, 085157 (2024).
- [27] Y.-Y. Zhang, R.-L. Chu, F.-C. Zhang, and S.-Q. Shen, Localization and mobility gap in the topological Anderson insulator, *Phys. Rev. B* **85**, 035107 (2012).
- [28] E. J. Meier, F. A. An, A. Dauphin, M. Maffei, P. Massignan, T. L. Hughes, and B. Gadway, Observation of the topological Anderson insulator in disordered atomic wires, *Science* **362**, 929 (2018).
- [29] Z.-W. Zuo and D. Kang, Reentrant localization transition in the Su-Schrieffer-Heeger model with random-dimer disorder, *Phys. Rev. A* **106**, 013305 (2022).
- [30] S.-N. Liu, G.-Q. Zhang, L.-Z. Tang, and D.-W. Zhang, Topological Anderson insulators induced by random binary disorders, *Phys. Lett. A* **431**, 128004 (2022).
- [31] W. Zhang, D. Zou, Q. Pei, W. He, J. Bao, H. Sun, and X. Zhang, Experimental Observation of Higher-Order Topological Anderson Insulators, *Phys. Rev. Lett.* **126**, 146802 (2021).
- [32] S. Velury, B. Bradlyn, and T. L. Hughes, Topological crystalline phases in a disordered inversion-symmetric chain, *Phys. Rev. B* **103**, 024205 (2021).
- [33] I. C. Fulga, B. van Heck, J. M. Edge, and A. R. Akhmerov, Statistical topological insulators, *Phys. Rev. B* **89**, 155424 (2014).
- [34] J. Zhang, Z.-Q. Zhang, S.-g. Cheng, and H. Jiang, Topological Anderson insulator via disorder-recovered average symmetry, *Phys. Rev. B* **106**, 195304 (2022).
- [35] R. Ma and C. Wang, Average Symmetry-Protected Topological Phases, *Phys. Rev. X* **13**, 031016 (2023).
- [36] S. Stützer, Y. Plotnik, Y. Lumer, P. Titum, N. H. Lindner, M. Segev, M. C. Rechtsman, and A. Szameit, Photonic topological Anderson insulators, *Nature* **560**, 461

- (2018).
- [37] G.-G. Liu, Y. Yang, X. Ren, H. Xue, X. Lin, Y.-H. Hu, H.-x. Sun, B. Peng, P. Zhou, Y. Chong, and B. Zhang, Topological Anderson Insulator in Disordered Photonic Crystals, *Phys. Rev. Lett.* **125**, 133603 (2020).
- [38] X. Cui, R.-Y. Zhang, Z.-Q. Zhang, and C. T. Chan, Photonic  $Z_2$  Topological Anderson Insulators, *Phys. Rev. Lett.* **129**, 043902 (2022).
- [39] L. Bunimovich and B. Webb, *Isospectral Transformations: A New Approach to Analyzing Multidimensional Systems and Networks* (Springer New York, 2014).
- [40] W. Barrett, A. Francis, and B. Webb, Equitable decompositions of graphs with symmetries, *Linear Algebra Appl.* **513**, 409 (2017).
- [41] C. Godsil and J. Smith, Strongly Cospectral Vertices, [arXiv:1709.07975](https://arxiv.org/abs/1709.07975) (2017).
- [42] D. Smith and B. Webb, Hidden Symmetries in Real and Theoretical Networks, *Physica A* **514**, 855 (2019).
- [43] M. Kempton, J. Sinkovic, D. Smith, and B. Webb, Characterizing cospectral vertices via isospectral reduction, *Linear Algebra Appl.* **594**, 226 (2020).
- [44] C. Morfonios, M. Pyzh, M. Röntgen, and P. Schmelcher, Cospectrality preserving graph modifications and eigenvector properties via walk equivalence of vertices, *Linear Algebra Appl.* **624**, 53 (2021).
- [45] M. Röntgen, N. E. Palaiodimopoulos, C. V. Morfonios, I. Brouzos, M. Pyzh, F. K. Diakonou, and P. Schmelcher, Designing pretty good state transfer via isospectral reductions, *Phys. Rev. A* **101**, 042304 (2020).
- [46] M. Röntgen, M. Pyzh, C. Morfonios, N. Palaiodimopoulos, F. Diakonou, and P. Schmelcher, Latent Symmetry Induced Degeneracies, *Phys. Rev. Lett.* **126**, 180601 (2021).
- [47] C. V. Morfonios, M. Röntgen, M. Pyzh, and P. Schmelcher, Flat bands by latent symmetry, *Phys. Rev. B* **104**, 035105 (2021).
- [48] M. Röntgen, X. Chen, W. Gao, M. Pyzh, P. Schmelcher, V. Pagneux, V. Achilleos, and A. Coutant, Topological states protected by hidden symmetry, *Phys. Rev. B* **110**, 035106 (2024).
- [49] L. Eek, Z. F. Osseweijer, and C. M. Smith, Fractality-induced topology, [arXiv:2411.12341](https://arxiv.org/abs/2411.12341) (2024).
- [50] A. Moustaj, L. Eek, M. Rontgen, and C. M. Smith, Latent Haldane Models, [arXiv:2411.08202](https://arxiv.org/abs/2411.08202) (2024).
- [51] L.-Y. Zheng, Y.-F. Li, J. Zhang, and Y. Huang, Robust topological edge states induced by latent mirror symmetry, *Phys. Rev. B* **108**, L220303 (2023).
- [52] L. Eek, M. Röntgen, A. Moustaj, and C. M. Smith, Higher-order topology protected by latent crystalline symmetries, [arXiv:2405.02704](https://arxiv.org/abs/2405.02704) (2024).
- [53] M. Röntgen, C. Morfonios, P. Schmelcher, and V. Pagneux, Hidden Symmetries in Acoustic Wave Systems, *Phys. Rev. Lett.* **130**, 077201 (2023).
- [54] L. Eek, A. Moustaj, M. Röntgen, V. Pagneux, V. Achilleos, and C. M. Smith, Emergent non-Hermitian models, *Phys. Rev. B* **109**, 045122 (2024).
- [55] H.-T. Hu, X. Lin, A.-M. Guo, Z. Lin, and M. Gong, Hidden self-duality in quasiperiodic network models, [arXiv:2411.06843](https://arxiv.org/abs/2411.06843) (2024).
- [56] H. C. Po, A. Vishwanath, and H. Watanabe, Symmetry-based indicators of band topology in the 230 space groups, *Nat. Commun.* **8**, 50 (2017).
- [57] H. Watanabe, H. C. Po, and A. Vishwanath, Structure and topology of band structures in the 1651 magnetic space groups, *Sci. Adv.* **4**, eaat8685 (2018).
- [58] B. Bradlyn, L. Elcoro, J. Cano, M. G. Vergniory, Z. Wang, C. Felser, M. I. Aroyo, and B. A. Bernevig, Topological quantum chemistry, *Nature* **547**, 298 (2017).
- [59] L. Elcoro, B. J. Wieder, Z. Song, Y. Xu, B. Bradlyn, and B. A. Bernevig, Magnetic topological quantum chemistry, *Nat. Commun.* **12**, 5965 (2021).
- [60] Z. Xiao, J. Zhao, Y. Li, R. Shindou, and Z.-D. Song, Spin space groups: Full classification and applications, *Phys. Rev. X* **14**, 031037 (2024).
- [61] X. Chen, J. Ren, Y. Zhu, Y. Yu, A. Zhang, P. Liu, J. Li, Y. Liu, C. Li, and Q. Liu, Enumeration and representation theory of spin space groups, *Phys. Rev. X* **14**, 031038 (2024).
- [62] Y. Jiang, Z. Song, T. Zhu, Z. Fang, H. Weng, Z.-X. Liu, J. Yang, and C. Fang, Enumeration of symmetries of magnetic orders, *Phys. Rev. X* **14**, 031039 (2024).
- [63] I. C. Fulga, F. Hassler, A. R. Akhmerov, and C. W. J. Beenakker, Scattering formula for the topological quantum number of a disordered multimode wire, *Phys. Rev. B* **83**, 155429 (2011).
- [64] S. Longhi, Topological anderson phase in quasi-periodic waveguide lattices, *Opt. Lett.* **45**, 4036 (2020).
- [65] A. MacKinnon and B. Kramer, The scaling theory of electrons in disordered solids: Additional numerical results, *Z. Physik B* **53**, 1 (1983).
- [66] R. Resta, Quantum-mechanical position operator in extended systems, *Phys. Rev. Lett.* **80**, 1800 (1998).
- [67] P. Duarte and M. J. Torres, Eigenvectors of isospectral graph transformations, *Linear Algebra Appl.* **474**, 110 (2015).
- [68] See Supplemental Material for the disordered trimerized chain, where the G1, and G0 are set as the lattice building block case of the intracell and intercell.
- [69] C.-A. Li, S.-B. Zhang, J. C. Budich, and B. Trauzettel, Transition from metal to higher-order topological insulator driven by random flux, *Phys. Rev. B* **106**, L081410 (2022).
- [70] C.-A. Li, B. Fu, J. Li, and B. Trauzettel, Random-flux-induced topological phase transitions and Chern insulators, [arXiv:2411.09780](https://arxiv.org/abs/2411.09780) (2024).

## Supplemental material for: Topological Anderson insulators by latent symmetry

### Trimerized chain with latent chiral symmetry

In the main texts, we have explained the TAIs of the prototype examples in terms of their latent chiral symmetry or inversion symmetry. Now we illustrate another more simple systems, the disordered trimerized chain, as shown in Fig.S1(a). In this case, the lattice building block for intracell is  $G_1$ , and  $G_0$  is the lattice building block for intercell. The tight-binding model of the trimerized model in real space can be described by

$$H_T = \sum_j^N (J_j c_{A,j}^\dagger c_{B,j} + t c_{B,j}^\dagger c_{C,j}) + \sum_j^{N-1} t c_{C,j}^\dagger c_{A,j+1} + h.c., \quad (\text{S1})$$

where  $t$  is the intercell hopping amplitude, whereas  $t$  and  $J_j$  are the intracell hopping amplitudes. The disorder is introduced in the intracell hopping  $J_j = J + W\omega_j$ , where  $\omega_j$  is random variables uniformly distributed in the interval  $[-1/2, 1/2]$ .

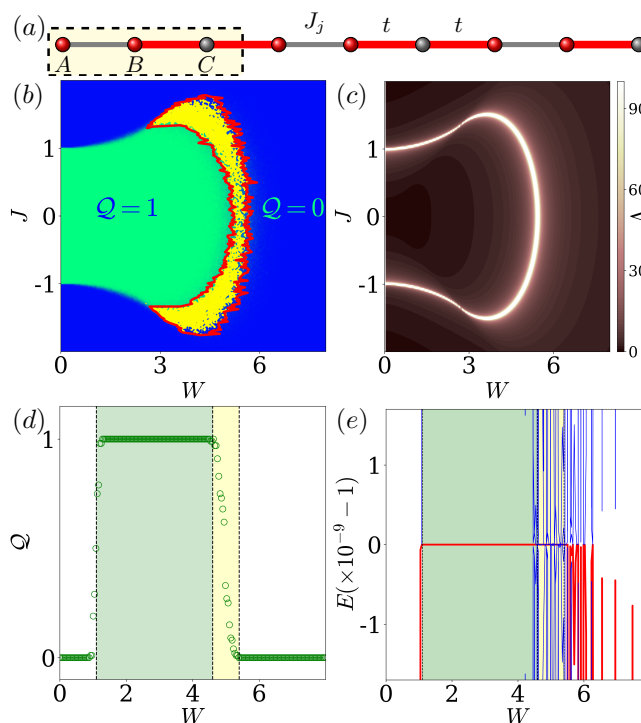


FIG. S1. (a) The lattice sites of the unit cell for the trimer chain are marked as  $A$ ,  $B$ , and  $C$ . The intercell hopping amplitude is  $t$ , and the intracell hopping amplitudes are  $J_j$  and  $t$ . (b) Disorder-averaged real-space topological number  $Q$  in the  $W - J$  plane for filling factor  $1/3$  with  $t = 1$ . (c) The white line is the topological phase boundary revealed by divergence of the localization length  $\Lambda$  of topological edge states. (d) Disorder-averaged topological number  $Q$  and (e) eigenvalues  $E$  as a function of  $W$  at the initial hopping amplitude  $J = 1.05$  of (b), where the number of unit cells is fixed as  $N = 2000$ . Here, the trivial phase, the gapped TAIs with bulk band gap, and the ungapped TAIs without bulk band gap are marked by white, green, and yellow shades, respectively.

The Hamiltonian of trimerized model does not have a chiral symmetry. Nevertheless, performing an ISR over the  $S = A, B$ , we obtain an energy-dependent on-site potential  $V = t^2/E$ , an intracell coupling  $a_j = J + W\omega_j$ , and an intercell coupling  $b_j = t^2/E$ . For disordered trimerized model under PBCs, the isospectral effective Hamiltonian can be changed to the mathematical form  $\hat{\mathcal{R}}_S(H_T) - VI$  of the disordered SSH model with chiral symmetry. In other words, this trimerized chain has latent chiral symmetry.



As discussed above, topological phase transitions are accompanied by divergence of the localization properties of the SSH model's eigenstates at zero energy modes. By applying Birkhoff's ergodic theorem, we can obtain inverse of the localization length of zero-energy states of the effective Hamiltonian  $\hat{\mathcal{R}}_S(H_T) - VI$  as:

$$\Lambda^{-1} = \left| \ln \left[ \frac{2t^2 |2J - W|^{(J/W - 1/2)}}{E |2J + W|^{(J/W + 1/2)}} \right] + 1 \right|. \quad (\text{S2})$$

In the following, we numerically show that the trimerized model with latent chiral symmetry features a quantized topological number  $\mathcal{Q}$ . By simulating the disorder-averaged real-space topological number  $\mathcal{Q}$  for the system of  $N = 200$  on the  $W - J$  plane over  $N_c = 100$  disorder configurations, we obtain the topological phase diagram shown in Fig.S1(b). Interestingly, there exists nontrivial  $\mathcal{Q} = 1$  phase in the green region with moderate disorder strength, indicating the existence of topological states induced by the disorder. The yellow region selected by the red solid line is the ungapped TAI phase which occupies a certain width. In Fig.S1(b,c), numerical calculations show that the topological phase transition revealed by the abrupt changes of real-space topological number  $\mathcal{Q}$  for PBCs and divergence of the localization length  $\Lambda$  for PBCs agree with each other.

In the clean limit ( $W = 0$ ), the critical condition for the topological phase transition is  $J = \pm 1$ . When  $J > 1$ , there will be a topological state plateau where  $\mathcal{Q} = 1$  induced by intermediate disorder. In Fig.S1(d), we take the evolution of  $\mathcal{Q}$  with disorder strength  $W$  at  $J = 1.05$ . It clearly reveals that disorder can induce TAI phase transition at  $W \approx 1.1$ , where the trivial band gap defined by the interval between the  $N$ th and  $(N + 1)$ th eigenvalues closes and reopens signaling the topological phase transition with the topological number  $\mathcal{Q}$  from zero to one. The system will maintain in the TAI phase until  $W \approx 5.4$ , and then return to the trivial phase due to strong disorder.

To provide a comprehensive view of the region for ungapped TAIs, that disorder-averaged value of the  $\mathcal{Q}$  is no longer quantized, we further analyze the eigenvalues as a function of the disorder strength  $W$  in Fig.S1(e) that the topological gap existing in the gapped TAI phase is closed in the ungapped TAI phase as the disorder strength increases. In the diagrams of the eigenvalue evolution, the  $N$ th eigenvalue closest to  $E_n = -1$  is highlighted with red lines, while the remaining eigenvalues with blue lines. The topological edge states are robust, which are transformed into the localized bulk states under strong disorder. As we introduce moderate disorder ( $4.6 \lesssim W \lesssim 5.4$ ), the band gap vanishes at the yellow shaded region of ungapped TAIs, and the  $(N - 1)$ th and  $(N + 1)$ th eigenvalues become degenerate. The topological edge states and the localized bulk states coexist stably in the ungapped TAIs. For the filling  $2/3$ , we can use the similar analysis to obtain the topological phase transitions. In short, the numerical simulations demonstrate the existence of the gapped and ungapped TAI phases with latent chiral symmetry induced by disorder.